In Situ Preparation of Oxide-Based Supported Catalysts by Solution Combustion Synthesis

Peter Dinka and Alexander S. Mukasyan*

Department of Chemical and Biomolecular Engineering, Center for Molecularly Engineered Materials, University of Notre Dame, Notre Dame, Indiana 46556

Received: August 10, 2005; In Final Form: September 19, 2005

The oxide-based supported catalysts with high specific surface area (>200 m^2/g) were produced in one step through combination of the impregnation and solution combustion synthesis approaches. As a model system, iron oxide was selected, which was loaded on different porous supports including α-Al_2O_3, γ-Al_2O_3, and ZrO_2, as well as activated alumina. It was shown that for the former three cases the specific surface areas of the supported catalysts are about or below the surface areas of the support. However, for the activated Al_2O_3 this characteristic significantly increases compared to that of the support. It was demonstrated that the developed approach may be used to produce different types of oxide-based supported catalysts, including perovskites.

Introduction

The oxides, including perovskites, are found to be an active catalysts for various reactions such as partial oxidation of methane[1] and steam reforming of methane[2] or heavy hydrocarbons,[3] in direct methanol[4] and high-temperature solid fuel cells.[5] It is known that the exact phase composition, types of structural defects, and high specific surface area are the main parameters which define catalyst properties.[6,7] Different approaches are used to synthesize oxides to fit the above requirements. Among them are precipitation and sol−gel methods, which produce powders with high specific surface area.[7−9] However, in both these techniques an additional heat treatment to obtain the desired phase composition and purity is typically required, which leads to significant material coarsening. In the other cases, the required reaction conditions (i.e. high temperatures) cause the same effect.[10]

In this paper we consider another method, which is based on the combustion phenomena, so-called Self-propagating High-temperature Synthesis (SHS).[11−13] In the conventional SHS scheme, the initial reaction medium is a mixture of particles with a size scale in the range 1−100 μm. After reaction initiation, this mixture burns at relatively high temperatures (>2000 K) in a self-sustained manner, forming the material of desired composition. The above features, while providing a rapid technique for the synthesis of powders with well-define crystalline structures, make it difficult to obtain *nanoscale* (high surface area) products.

A combination of SHS and reactive solution approaches[14,15] leads to the so-called solution (or aqueous) combustion synthesis (SCS) method.[16−22] This process typically involves a reaction in solution of metal nitrates and different fuels, which can be classified based on their chemical structure, i.e., type of reactive groups (e.g., amino, hydroxyl, carboxyl) bonded to the hydrocarbon chain. These fuels reacting with oxygen-containing species, formed during the nitrates decomposition, provide rapid high-temperature interaction in the system. More specifically, after preheating to moderate temperatures (~150−200 °C), the reaction can be initiated and the combustion front propagates in a self-sustained manner through the system, leaving behind fine solid product of tailored composition.

Several SCS features contribute to the unique properties of the synthesized powders. First, being the liquid state the initial reaction media (e.g., aqueous solution) allows mixing of the reactants on the molecular level, thus permitting precise and uniform formulation of the desired composition on the nanoscale. Second, the high SCS temperature (>900 °C) ensures high product purity and crystallinity. The latter allows one to skip the additional high-temperature calcination step typically followed in conventional approaches. Third, short process duration (ca. seconds) and formation of various gas-phase products during the high-temperature combustion reaction inhibit particle size growth and favor the formation of nanosize powders with high specific surface area. All of the above characteristics make solution combustion especially attractive for the synthesis of a variety of *catalysts*, which as mentioned above, require precise phase composition and high specific surface area.

Solid catalysts[9] (e.g., metal oxide) are typically prepared from fine powders to provide the highest specific surface area for effective reaction. In some cases active material is dispersed over a less active porous substance called a support. The advantages of such supported catalysts are easy catalyst recovery, increased activity, decreased amount of expensive active material required, and enhanced mechanical properties. Many such supported catalysts are produced by impregnation, which consists of repeated dipping of porous support pellets into a solution containing a desired catalytic agent. Various techniques such as pressurizing, vacuum treatment, acoustic activation, etc. are used to facilitate the impregnation process. They, however, are expensive and long duration processes.

Several publications are available on the preparation of the supported catalyst by utilization of the solution combustion approach (cf. refs 23−28). However, none of them reported synthesis of such catalyst in controllable combustion mode in one step. More importantly, the critical fundamental issues related to the influence of combustion parameters and support nature on the properties (phase composition and specific surface area) of the synthesized materials were not addressed in these researches. In this work we demonstrated that supported catalysts with exceptionally high specific surface area (>200 m^2/g) can

* To whom correspondence should be addressed. Phone: (574) 631-9825. Fax: (574) 631-8366. E-mail: amoukasi@nd.edu.

10.1021/jp054486n CCC: $30.25
Published on Web 10/26/2005

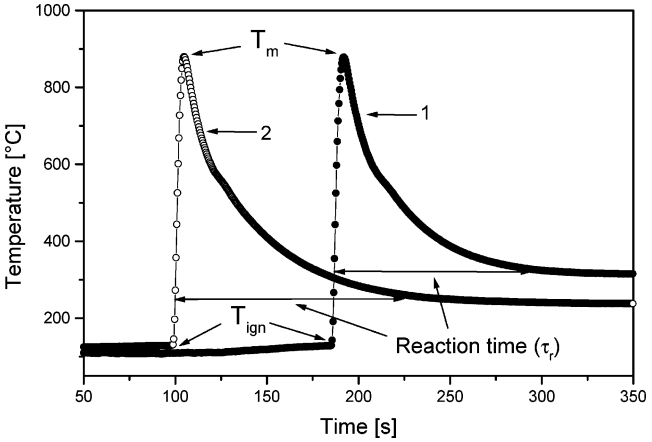

Figure 1. Temperature−time history of the solution combustion in a iron nitrate−glycine system ($\phi = 1$) with (curve 1) and without (curve 2) water addition.

be prepared in a controlled manner in one step through a combination of the impregnation and solution combustion approaches. The fundamental aspects of the influence of synthesis conditions on product microstructure were investigated. Iron oxide loaded on different solid supports, including α- and γ-Al_2O_3, ZrO_2, as well as activated alumina, was selected as a model system. Note, that iron oxide is the active catalyst for a variety of reactions, such as toluene ammoxidation,[29] conversion of syngas to light olefins,[30] or the Fischer−Tropsch reaction.[31]

Experimental Section

Ferric nitrate, $Fe(NO_3)_3 \cdot 9H_2O$ (98%, Alfa Aesar; bp125 °C), was used as a basic oxidizer and glycine, $CH_2NH_2CO_2H$ (98%, Alfa Aesar; mp 262 °C), as a fuel. Under equilibrium conditions, the reactions in these systems can be represented as follows:

$$Fe(NO_3)_3 + 5/3 \cdot \phi CH_2NH_2CO_2H + 15/4(\phi - 1)O_2 \Rightarrow 1/2Fe_2O_3(s) + 10/3 \cdot \phi CO_2(g) + 25/6 \cdot \phi H_2O(g) + (5/3 \cdot \phi + 3)/2N_2(g)$$

where $\phi = 1$ means that the initial mixture does not require atmospheric oxygen for complete oxidation of fuel, while $\phi > 1$ (< 1) implies fuel-rich (lean) conditions.

A chemical reactor made of quartz (cf. ref 21) allows one to conduct experiments in different ambient atmospheres (i.e., air, oxygen, argon) and process monitoring by using a digital camera (Panasonic Digital Camcorder, Model PV-DV103). The reaction temperature−time history was recorded by a set of thermocouples (125/250 μm, type K, Omega Engineering), using a computer equipped with a multichannel acquisition system (INET-200 controller card, Omega Engineering Inc.) with rates ranging from 5 to 60 samplings per second.

Powder Catalyst Preparation. To synthesize powder catalyst, the reactor containing the prepared solution was placed on a hot plate (Cole Parmer model 4803-00) and the mixture was preheated uniformly. Unlike conventional solution combustion,[21] in this work the fuel and oxidizer were mixed without the addition of water. It appears that crystalline water attached to the iron nitrate was released upon contact with the glycine forming a homogeneous, viscous mixture. This approach avoids the relatively long stage of additional water evaporation. The typical temperature−time histories of the SCS process with (curve 1) and without (curve 2) water addition are shown in Figure 1. It can be seen that at the so-called ignition temperature ($T_{ig} \sim 130$ °C) the reaction initiates and proceeds at extremely high rate reaching a maximum temperature value $T_m \sim 900$ °C. The process duration time is in the range $10-10^2$ s. In general, the process temperature profile depends on the experimental conditions (e.g., ratio between fuel and oxidizer, ϕ; local mixture ignition; nature of the fuel; etc.).

TABLE 1: Properties of Support Materials

support	form	surface area [m^2/g]	density [g/cm^3]	vendor
α-Al_2O_3	1−2 mm spheres	5	3.97	Alfa Aesar
γ-Al_2O_3	3 mm pellets	244	3.97	Alfa Aesar
ZrO_2	3 mm pellets	125	5.89	Alfa Aesar
activated Al_2O_3	1.4−2.4 mm grains	149	4.0	Fisher Sci.

Supported Catalyst Preparation. The characteristics of all materials used as a support are presented in Table 1. The desired amount of porous support pellets was added to the reaction solution (e.g., mixture of glycine and iron nitrate). A parameter, η, which defines the ratio between the amount of support particles and iron oxide product, is important in investigated conditions ($\eta = 0$, a mixture without support or $\eta = 1$, e.g., reactants weighed for the synthesis of 1 g of Fe_2O_3 are mixed with 1 g of support particles). The prepared heterogeneous reaction media was preheated to $T_{ig} \sim 130$ °C at which point the mixture was self-ignited and burned. Reaction products involve two parts: iron oxide powder and iron oxide dispersed over the support. After cooling, these products were separated by sieving. The obtained products were analyzed for phase composition and crystallinity with use of a X1 Advanced Diffraction System (Scintag Inc., USA). The powder microstructure was studied by field emission scanning electron microscopy (LEO, series EVO 50, equipped with EDS) and the specific surface area was measured by using BET analysis (Autosorb1C, Quantachrome Inst.). Finally, differential thermal/thermogravimetric data on the precursor's decomposition were obtained with a DTA/TGA analyzer (model SDT 2960, TA Inst.).

Results

Synthesis. The typical time−temperature profiles of the solution CS process for the mixtures without ($\phi = 1$, $\eta = 0$, curve 1) and with different catalyst supports ($\phi = 1$; $\eta = 1$, curves 2−5) are shown in Figure 2. In all cases, the temperature slowly increases up to T_{ig}, where it sharply rises (dT/dt up to 120 °C/s) to the maximum T_m value. It can be seen that the presence of the support does not influence T_{ig}, which is ∼128 ± 4 °C and as is related to the rapid reaction between HNO_3 species (which formed due to hydrolysis of iron nitrate) and glycine.[21] Contrarily, the maximum reaction temperature (T_m) and duration of the high-temperature zone (τ_r) both depend on the type of added support. For a "pure" mixture ($\eta = 0$) these parameters are $T_m = 880$ °C and $\tau_r = 140$ s. In the mixtures with supports T_m varies for different materials being 640, 620, and 520 °C for γ-Al_2O_3, α-Al_2O_3, and ZrO_2 supports, respectively. It is important that a significant decrease in maximum combustion temperature was observed for activated alumina, $T_m = 310$ °C. The synthesis time, τ_r, typically increases with increasing T_m, owing to the longer postcombustion region. However, the τ_r value for the activated Al_2O_3 system appeared to be the largest among the investigated systems, despite the lowest maximum reaction temperature (see Discussion for details).

The influence of the η parameter for activated alumina support on the temperature−time history of the synthesized process is

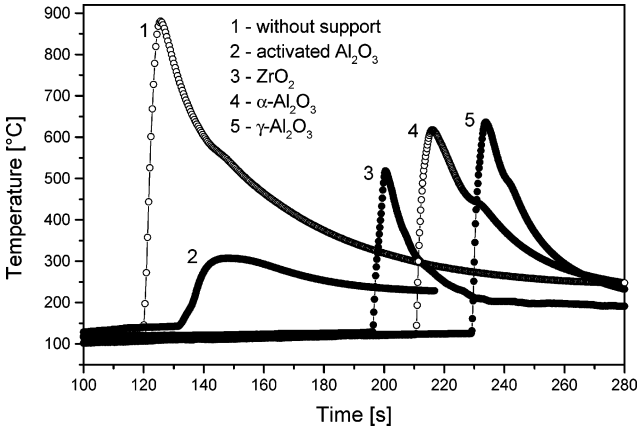

Figure 2. Temperature profiles of the solution combustion in different iron nitrate−glycine solid support systems ($\phi = 1$; $\eta = 1$).

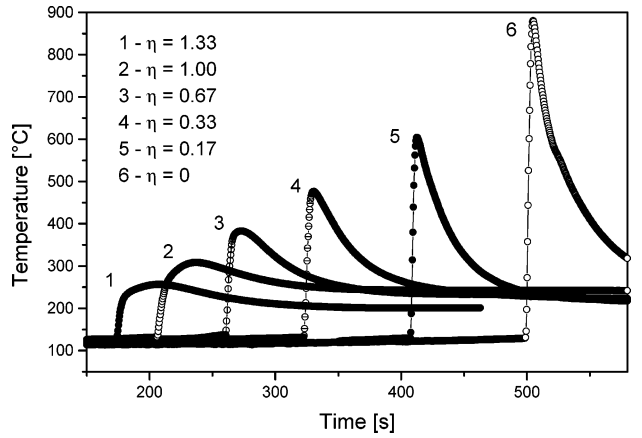

Figure 3. Temperature profiles of the solution combustion in a iron nitrate−glycine activated Al_2O_3 system with different amounts of added support (parameter η).

shown in Figure 3, and indicates that T_m monotonically decreases with increase in the amount of added "inert" support (Figure 4a), while T_{ig} remains essentially constant (Figure 4b). Note that in Figure 3 graphs have been purposely plotted so as to have the data of the six curves fit in an orderly way into one graph. Thus the "initiation" points (i.e., at which the dT/dt sharply rises) along the time axis do not reflect the real ignition delay time.

Product Characterization. Two types of products were obtained, i.e., powdered iron oxide and supported iron oxide catalysts. Properties of these products are presented in Tables 2 and 3. First, it can be seen that the addition of a support into the solution ($\eta > 0$) increases the iron oxide powder surface area as compared to "pure" mixture conditions ($\eta = 0$; $S = 1.9$ m^2/g). Second, the specific surface area (S) of the supported catalysts changes differently with respect to the S of the initial supports (Table 2), i.e., decreases for γ-Al_2O_3 and ZrO_2, only slightly increases for α-Al_2O_3, and significantly rises for activated Al_2O_3. Also it was shown that while an average pore size for all supports remains constant, the cumulative pore volume changes after combustion, leading to particularly distinct increases for activated Al_2O_3 (Table 3). The XRD and EDS analysis reveals that all synthesized catalysts are pure γ-Fe_2O_3.

The above-mentioned data allow one to conclude that the highest surface area of both powder and supported catalysts was obtained by using activated alumina. For these reasons, we further focused on the results obtained with this type of support.

Activated Alumina. To explain the significantly higher surface area (>200 m^2/g) of the loaded support as compared to

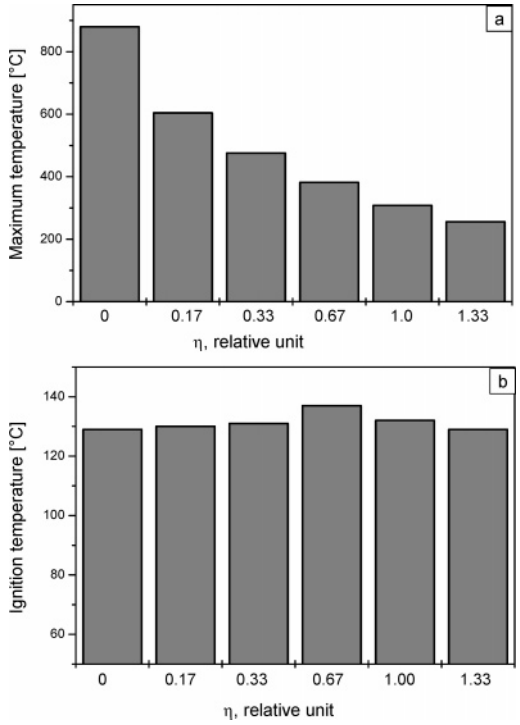

Figure 4. Dependences of maximum combustion (a) and ignition (b) temperatures on the ratio between support material and iron oxide product (iron nitrate−glycine activated Al_2O_3 system).

TABLE 2: Specific Surface Areas of Different Initial Supports and Combustion Products ($\phi = 1$ and $\eta = 1$)

support	surface area of initial support [m^2/g]	surface area of iron oxide powder[a] [m^2/g]	surface area of supported catalyst [m^2/g]
Al_2O_3 activated	149	40	225
α-Al_2O_3	5.1	4.5	5.8
γ-Al_2O_3	244	37	197
ZrO_2	125	22	112

[a] Specific surface area of "pure" iron oxide powder ($\eta = 0$) is 1.9 m^2/g.

TABLE 3: Microstructural Characteristics of Initial Supports and Combustion Products ($\phi = 1$ and $\eta = 1$)

	cumulative pore volume [cm^3/g]		medium pore width [Å]	
support	pure support	loaded support	pure support	loaded support
Al_2O_3 activated	0.043	0.068	5	5
α-Al_2O_3	0.002	0.003	6.5	6
γ-Al_2O_3	0.086	0.080	5.5	5

an initial S of ~150 m^2/g for activated alumina, some additional experiments were conducted. It is known that activated Al_2O_3 is a hydrated alumina oxide, and water released during heat treatment may change the support microstructure leading to an increase in its surface area.[32] To verify this effect, the pure activated alumina support was calcined for 2 h in air at different temperatures, i.e., 200, 400, 600, and 800 °C. It was shown that no increase in S was observed. On the contrary, this thermal treatment caused a decrease of support specific surface area with increasing temperature: $S_{200} = 122$; $S_{400} = 116$; $S_{600} = 107$; $S_{800} = 74$ m^2/g, respectively.

However, used calcination conditions are different as compared to those for the SCS process. Thus, then the "inert" heat treatment of the support was conducted in the SCS wave. The activated alumina particles were covered by thin aluminum foil

TABLE 4: Specific Surface Area of Pure and Loaded Alumina Activated Support after Different Heat Treatments ($\eta = 1$, $\phi = 1$)

type of material	treatment	surface area [m^2/g]
activated Al_2O_3	original	149
activated Al_2O_3	calcined (800 °C, 2 h)	74
iron oxide loaded on original alumina	as synthesized	232
iron oxide loaded on original alumina	calcined (800 °C, 2 h)	129
iron oxide loaded on calcined alumina	as synthesized	221

and immersed in a standard iron nitrate−glycine solution ($\phi = 1$), which was then ignited. In this case the support was isolated from the chemical environment, but was heat treated in SCS-like conditions. It appears that after such rapid high-temperature (~1000 K) treatment the surface area of activated alumina remains essentially constant (144 m^2/g). It can be concluded that the hypothesized effect of Al_2O_3 microstructure transformation by heat treatment cannot cause the observed increase in supported catalyst surface area.

As was shown above, after calcination in air at $T = 800$ °C for 2 h, the surface area of the activated alumina supports decreases by half (from 149 to 74 m^2/g). However, the specific surface area of the two supported catalysts prepared in the combustion wave by using original and calcined supports appear to be essentially equal (232 and 221 m^2/g, respectively; see Table 4). It suggests that the BET method indeed characterizes only the surface of the supported catalyst that was formed during combustion reaction. This is confirmed by the fact that after 2 h of calcination at $T = 800$ °C loaded catalyst surface area (129 m^2/g) remains much higher than that for the original pure support after the same calcination procedure (74 m^2/g). Note that the S of the powder catalyst is much lower than that of the supported one. Thus, it can be concluded that the high specific surface area of the catalyst loaded on the activated Al_2O_3 is the result of the support−catalyst interaction occurring during formation of the iron oxide layer on the solid surface and is related to the specific nature of the solid material used.

TGA/DTA Analysis. In the above context, it is important to know what kind of transformations take place during heat treatment of the support in air. The TGA-DTA results for the original activated alumina, as well as those of the supported catalyst, are shown in Figure 5. For the original support (curve 1), the weight change in the range 100−150 °C relates to the loss of adsorbed water: the corresponding endotherm transformation can be seen on DTA curve 3. The weight loss at higher temperature (200−550 °C) occurs due to the release of the chemically bonded water, which is part of the activated alumina structure.[32] Overall weight loss is about 16 wt %. The TGA curve of loaded support (curve 2) shows a more smooth decrease of weight in the range 100−600 °C and the overall weight loss is 11.5 wt %. This suggests that part of the water was released from the support during the combustion reaction.

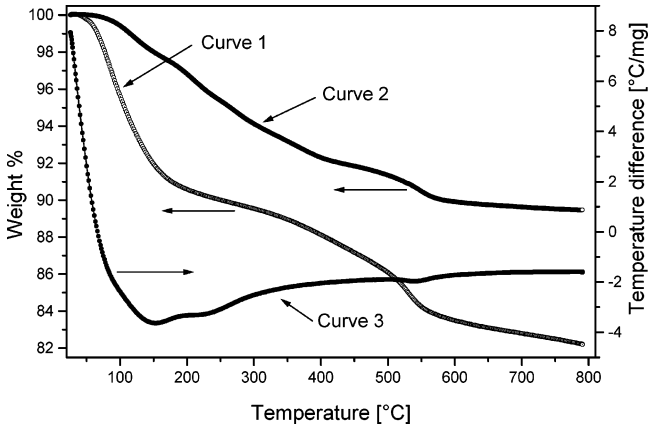

Figure 5. TGA/DTA data for activated Al_2O_3-based system: curves 1 and 3, TGA and DTA for original support, respectively; curve 2, TGA for supported catalyst.

TABLE 5: Specific Surface Area of Loaded Activated Al_2O_3 Supports and Iron Oxide Powders at Different ϕ and η

factor η	surface area of supported catalyst [m^2/g]	surface area of powder catalyst [m^2/g]
	$\phi = 1$	
0	149	1.9
1/6	197	3.0
1/3	219	8.5
2/3	222	22
1	232	33
4/3	222	35
	$\phi = 3$	
1/3	211	25

Reaction Mixture Composition and Catalyst Characteristics. The surface areas of the original activated Al_2O_3 support and "pure" ($\eta = 0$) iron oxide powder are 149 and 1.9 m^2/g, respectively. It can be seen from Table 5 that under a stoichiometric proportion of fuel and oxidizer ($\phi = 1$), the surface area of supported catalyst rapidly increases with increasing degree of dilution, η, and achieves saturation at $\eta = 1$ (232 m^2/g). The surface area of iron oxide powder, synthesized during the same experiments, monotonically increases with increasing η. Similar trends were found for other supports: for example, for the γ-Al_2O_3 case, the surface area of both the support and the powder catalysts increased from 197 ($\eta = 1$) to 208 ($\eta = 3$) and 37 ($\eta = 1$) to 44 ($\eta = 3$) m^2/g, respectively. However, the S for supported catalysts was lower as compared to the initial value for γ-Al_2O_3 (244 m^2/g).

Another observed effect, i.e., increase of fuel-to-oxidizer ratio, ϕ, leads to increase in surface area of the powder-type catalyst (e.g. $S_p(\phi=1) = 8.5$ m^2/g and $S_p(\phi=3) = 25$ m^2/g), is in qualitative agreement with previously obtained results.[21] However, the S of the supported catalysts remains essentially constant for different solution compositions (e.g., $S_p(\phi=1;\eta=1/3) = 219$ m^2/g and $S_p(\phi=3;\eta=1/3) = 211$ m^2/g).

Microstructures. An important characteristic of the supported catalyst is an active phase distribution along the support surface and its bulk.[33] To investigate this matter a detailed microstructural analysis of the synthesized catalysts was conducted. The statistical EDS analysis along the relatively large (100 μm × 100 μm) areas (so-called elemental mapping) showed that iron is uniformly distributed along the surface of the support. The elemental microanalysis of the supported catalyst cross section was also performed. The typical cross sections of the supported catalysts are shown in Figure 6. The elemental microanalysis along the line, which connects the particle surface and its center, reveals the existence of a relatively thick layer where iron was unequivocally detected (e.g., points 1−4 in Table 6). The iron concentration drops abruptly to zero on the inside boundary of the layer (e.g., points 5 and 6 in Table 6). The thickness of the layer varies for different supports, e.g., being ~120 μm for activated Al_2O_3 (Figure 6b) and ~30 μm for α and γ (Figure 6a) alumina. Additional layer-by-layer EDS and XRD analysis showed that (a) the ratio between weight concentration of the major elements, i.e., Fe:Al:O, remains essentially constant through the entire thickness of the catalytic layer (30−120 μm)

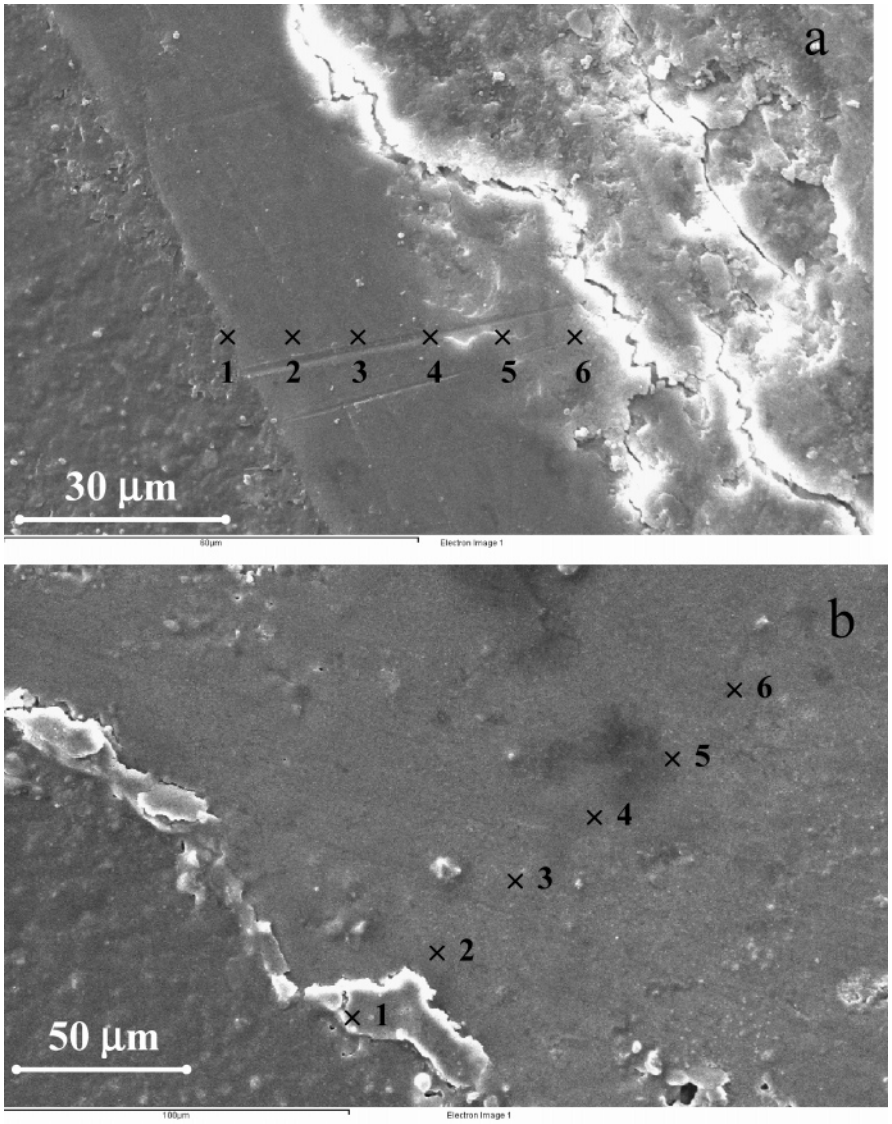

Figure 6. Typical cross sections for catalysts loaded on different supports: (a) γ-Al_2O_3 and (b) activated Al_2O_3.

TABLE 6: The Elements of Distribution along the Supported Catalysts[a]

	γ-Al_2O_3 support		activated Al_2O_3	
points	Al [wt %]	Fe [wt %]	Al [wt %]	Fe [wt %]
1	50.6	3.8	41.4	10.9
2	49.9	4.5	47.4	8.2
3	50.4	3.7	47.8	8.5
4	50.1	4.2	45.9	10.3
5	52.9	0	52.9	0
6	52.9	0	52.9	0

[a] Balance is oxygen.

and (b) only two phases, Al_2O_3 (ZrO_2) and γ-Fe_2O_3, were detected. These results allowed us to conclude that γ-Fe_2O_3 (+3 oxidation level) is uniformly distributed along the layer.

Discussion

The combustion mechanism in the glycine−iron nitrate system was discussed in our previous work.[21] It is expected that the general reaction scheme does not change when the "inert" solid substance is added to the system. This conclusion is supported by the facts that self-ignition temperature does not depend on the amount of diluent (i.e., parameter η; see Figure 4b) and the specific surface area of the products is higher for the fuel-rich ($\phi > 1$; see Table 5) mixtures.[21,22] It is also obvious that maximum reaction temperature (T_m) decreases with increasing η (Figure 4a). The adiabatic combustion temperature in diluted systems can be calculated as follows: $T_{ad} \approx T_o + Q/c_p\rho(1 + \eta)$, where ρ and c_p are the mixture density and heat capacity and Q is a reaction heat per solution volume. This relation predicts that adding more inert substance to the reaction system (larger η) will lower the combustion temperature.

However, the data obtained on different supports (Figure 2) show the trends, which cannot be described by the above formula. Indeed, three systems with the same amount of different supports (η=1), i.e., α- and γ-Al_2O_3 and ZrO_2, possess similar T_m, while the activated Al_2O_3-based system reacts at much lower temperature. This effect can be explained by an additional endothermic process that occurs during the synthesis, which causes the temperature decrease. DTA analysis of the activated Al_2O_3 (Figure 5) allows us to identify such endothermic transformation, which is related to water desorption, at a temperature range of 100−300 °C. This process diminishes the T_m and also leads to an increase in the amount of gas-phase products on the support surface, where formation of the catalyst layer occurs. On the basis of the above data one can explain the observed unique effect of the extremely high surface area of the catalyst loaded on the activated alumina surface.

As was previously shown,[21,22] the decrease of reaction temperature and intensification of gas-phase evolution in the combustion wave lead to an increase in the product surface area. The former hinder kinetics of the nucleus growths and the latter prevents the collision between formed solid nuclei. During the combustion process, when temperature exceeds 100 °C, water starts to evaporate from the bulk of the activated Al_2O_3, providing specific conditions, i.e., low temperatures and intensive gas flow on the support surface. Under these conditions, the growth rate of iron oxide nuclei, which are formed in the vicinity of such a solid surface, is low. Taking into account the short reaction time during the combustion process (several seconds) it becomes clear why the synthesized supported catalyst has a high specific surface area. Thus this alumina support plays an active role in the process of microstructural transformation of the loaded catalyst. For other really inert substances (α- and γ-Al_2O_3 and ZrO_2), the surface areas of the loaded catalysts are slightly below the surface area of the original support (Tables 1 and 2). It means that the formed oxide "epitaxially" covered the surface of the support and sintering at high combustion temperature decreases the surface areas.

It is also important that the pure iron oxide was not observed on the support surface. The presence of all three elements (i.e., Al−Fe−O) was detected by the EDS microanalysis along the entire active layer thickness. It suggests that reaction solution penetrates inside the fine microstructure of the support and reaction combustion occurs in this porous media. The depth of iron oxide penetration varies for different supports and is much larger for activated Al_2O_3 (∼120 μm) as compared to other supports (30 μm) (Figure 6a,b). This effect cannot be directly related to the microstrutural characteristics of the support material. For example, γ-Al_2O_3 has a higher cumulative pore volume than activated alumina, but smaller depth of catalyst penetration (Table 3). It can be assumed that water, released during synthesis from the activated support, creates an extremely fine pore structure, which is then occupied by the catalyst phase. Additional experiments on controlling the catalyst distribution along the support are currently under investigation.

Thus, the active nature of a specially prepared support involves several important functions: (i) decreased reaction temperature; (ii) additional gas-phase evolution; and (iii) formation of fine pore -structures. These features lead to the formation of a supported catalyst with high (>200 m^2/g) surface area, which is stable enough to keep its fine microstructure after high-temperature calcinations. Finally, we applied the comprehensive combustion-impregnation approach to synthesize other oxide-based catalysts, including perovskites (e.g., the $LaFe_xNi_{1-x}O_3$ family). These systems result in a supported catalyst specific surface area of ∼175 m^2/g, which is much higher than that for powder CS product (∼30 m^2/g), as well as for original support (149 m^2/g).

To illustrate the activity of supported catalysts prepared by the direct combustion method the catalyst with $LaFe_{0.6}Ni_{0.4}O_3/Al_2O_3$ composition was tested in the auto-thermal steam reforming reaction of heavy hydrocarbons. This process is a promising hydrogen source for fuel cell applications.[34] The specially prepared surrogate was used as a fuel, the composition of which was calculated by a Computer Aided Reduction Method[35] to model JP-8 fuel, containing dodecane (34.7%), 1-decene (32.6%), methylcyclohexane (16.7%), and *tert*-butyl benzene (16.0%). The experiments were performed in a fixed bed reactor made of a quartz tube (7 mm i.d.) placed in an electrically heated furnace with precise temperature control in the vicinity of the catalyst location. The 0.5 g of catalyst was initially activated in a flow of nitrogen−hydrogen (5%) gas mixture (overall flow rate of 80 mL/min) at 800 °C for 2 h.

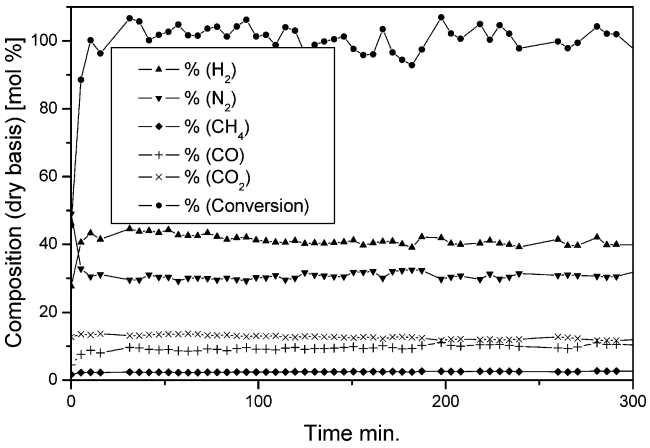

Figure 7. Product gas composition and reaction conversion obtained during steam reforming of JP-8 surrogate.

The fuel and water were evaporated prior to entering the reactor and mixed with air. The reactions proceed under the following conditions: atmospheric pressure, temperature 800 °C, fuel feeding rate ∼3 mL/h, and carbon/steam ratio = 3. To ensure the auto-thermal conditions ($O_2/C = 0.3518$) the airflow rate was ∼110 mL/min. Note that the above experiments were conducted with relatively high gas hourly space velocity (GHSV $=140\,000\ h^{-1}$). The reaction products were cooled and condensed water as well as higher hydrocarbons (if any) were trapped by a condenser. The rest of the gas effluent was analyzed by a two channel micro GC (Agilent Micro GC 3000A) equipped with thermoconductive detectors, using a molecular sieve and a Plot Q column with argon and helium as carrier gases, respectively.

Nitrogen in the air supplied to the reactor was used as a basis to determine the total carbon concentration in the effluent. The reaction conversion was calculated by dividing the sum of carbon in gaseous product (i.e., CO, CO_2, and CH_4) by carbon in the surrogate. The composition and fuel conversion of typical products are shown in Figure 7. It can be seen that full conversion (∼100%) was maintained during the duration of the experiments (12 h) and hydrogen concentration is close to the thermodynamically predicted theoretical limit (42 vol %). Detailed studies on the activities of different catalysts are currently under investigation.

Thus, in this work we the formulated fundamental basis on the so-called combustion-impregnation approach for synthesis of high-surface area supported catalysts. The formulated concept of "active" support is an attractive instrument for the synthesis of a variety of advanced materials.

Acknowledgment. This work was supported by the U.S. Army CECOM RDEC through Agreement AAB07-03-3-K414. Such support does not constitute endorsement by the U.S. Army of the views expressed in this publication.

References and Notes

(1) Provendier, H.; Petit, C.; Estournes, C.; Libs, S.; Kiennemann, A. *Appl. Catal. A* **1999**, *180*, 163.

(2) Provendier, H.; Petit, C.; Kiennemann, A. *Acad. Sci. Paris, Ser., Chim./Chem.* **2001**, *4*, 57.

(3) Kramarz, K. W.; Bloom, I. D.; Kumar, R.; Ahmed, S.; Wilkenhoener, R.; Krumpelt, M. U.S Patent 5,929,286, 2001.

(4) Martínez-Juárez, A.; Sánchez, L.; Chinarro, E.; Recio, P.; Pascual, C.; Jurado, J. R. *Solid State Ionics* **1999**, *135*, 163.

(5) Simner, S. P.; Bonnett, J. F.; Canfield, N. L.; Meinhardt, K. D.; Shelton, J. P.; Sprenkle, V. L.; Stevenson, J. W. *J. Power Sources* **2003**, *113*, 1.
(6) Twigg. M. V. *Catalyst Handbook*, 2nd ed.; Wolfe Publishing Ltd.: London, UK, 1989.
(7) Wang, C. H.; Chen, C. L.; Weng, H. S. *Chemosphere* **2004**, *57*, 1131.
(8) Schmidt, F. *Appl. Catal. A* **2001**, *221*, 15.
(9) Perego, C.; Villa, P. *Catal. Today* **1997**, *34*, 281.
(10) Escandón, L. S.; Ordóñez, S.; Vega A.; D×c6íez, F. V. *Chemosphere* **2005**, *58*, 9.
(11) Munir, Z. A.; Anselmi-Tamburini, U. *Mater. Sci. Rep.* **1989**, *3*, 277.
(12) Moore, J. J.; Feng, H. J. *Prog. Mater. Sci.* **1995**, *39*, 243.
(13) Varma, A.; Rogachev, A. S.; Mukasyan, A. S.; Hwang, S. *Adv. Chem. Eng.* **1998**, *24*, 79.
(14) Pechini, M. U.S. Patent 3,330,697, 1967.
(15) Androulakis, J.; Katsarakis, N.; Giapintzakis, J.; Vouroutzis, N.; Pavlidou, E.; Chrissafis, K.; Polychroniadis, E. K.; Perdikatsis, V. *J. Solid State Chem.* **2003**, *173*, 350.
(16) Kingsley, J. J.; Patil, K. C. *Mater. Lett.* **1988**, *6*, 427.
(17) Chick, L. A.; Pederson, L. R.; Maupin, G. D.; Bates, J. L.; Thomas, L. E.; Exarhos, G. J. *Mater. Lett.* **1990**, *10*, 6.
(18) Patil, K. C.; Aruna, S. T.; Ekambaram, S. *Curr. Opin. Solid State Mater. Sci.* **1997**, *2*, 158.
(19) Patil, K. C.; Aruna, S. T.; Mimani, T. *Curr. Opin. Solid State Mater. Sci.* **2002**, *6*, 507.
(20) Mukasyan, A. S.; Costello, C.; Sherlock, K. P.; Lafarga, D.; Varma, A. *Sep. Purif. Technol.* **2001**, *25*, 117.
(21) Deshpande, K.; Mukasyan, A.; Varma. A. *Chem. Mater.* **2004**, *16*, 4896.
(22) Varma, A.; Mukasyan, A. S.; Deshpande, K. T.; Pranda, P.; Erri, P. *Mater. Res. Soc. Symp. Proc.* **2004**, *800*, 113.
(23) Gonzalez-Cortes, S. L.; Xiao, T. C.; Costa, P. M. F. J.; Fontal, B.; Green, M. L. H. *Appl. Catal. A* **2004**, *270*, 209.
(24) Alifanti, M.; Blangenois, N.; Florea, M.; Delmon, B. *Appl. Catal. A* **2005**, *280*, 255.
(25) Isupova, L. A.; Alikina, G. M.; Tsybulya, S. V.; Salanov, A. N.; Boldyreva, N. N.; Rusina, E. S.; Ovsyannikova, I. A.; Rogov, V. A.; Bunina R. V.; Sadykov, V. A. *Catal. Today* **2002**, *75*, 305.
(26) Bera, P.; Priolkar, K. R.; Gayen, A.; Sarode, P. R.; Hegde, M. S.; Emura, S.; Kumashiro, R.; Jayaram, V.; Subbanna, G. N. *Chem. Mater.* **2003**, *15*, 2049
(27) Priolkar, K. R.; Bera, P.; Sarode, P. R.; Hegde, M. S.; Emura, S.; Kumashiro, R.; Lalla, N. P. *Chem. Mater.* **2002**, *14*, 2120.
(28) Bera, P.; Patil, K. C.; Jayaram, V.; Subbanna, G. N.; Hegde, M. S. *J. Catal.* **2000**, *196*, 293.
(29) Rombi, E.; Ferino, I.; Monaci, R.; Picciau, C.; Solinas, V.; Buzzoni, R. *Appl. Catal. A* **2004**, *266*, 73.
(30) Das, D.; Ravichandran, G.; Chakrabarty, D. K. *Catal. Today* **1997**, *36*, 285.
(31) Yang, Y.; Xiang, H. W.; Xu, Y. Y.; Bai, L.; Li, Y. W. *Appl. Catal. A* **2004**, *266*, 181.
(32) Mistra, C. *Industrial Alumina Chemicals*; American Chemical Society: Washington, DC, 1986.
(33) Morbidelli, M.; Gavriilidis, A.; Varma, A. *Catalyst Design*; Cambridge Univiersitty Press: New York, 2001.
(34) Suzuki, T.; Iwanami, H.; Yoshinary, T. *Int. J. Hydrogen Energy* **2000**, *25*, 119.
(35) Montgomery, C. J.; Cannon, S. M.; Mawid, M. A.; Sekar, B. 40th AIAA Aerospace Sciences Meeting and Exhibit, January 14−17, 2002, Reno, Nevada.